Influence of the production method on the thermophysical properties of high temperature molten salt-based nanofluids

Nuria Navarrete, Leonor Hernández, Antonio Vela, Rosa Mondragón*

Departamento de Ingeniería Mecánica y Construcción, Universitat Jaume I, 12071-Castellón de la Plana, Spain

**Corresponding author: mondragn@uji.es*

ABSTRACT

The potential use of molten salt-based nanofluids as thermal energy storage material in Concentrated Solar Power plants has gained attention over the last years due to their enhanced storage capacity. The possible effects of the salt-based nanofluid production at industrial scale has not been yet investigated, as this could influence the nanoparticles agglomeration and therefore their thermal and flow properties. Four methods were evaluated for the production of solar salt-based nanofluids containing 1 wt.% of silica nanoparticles. The particle size distribution, the stability, the rheological behaviour and the specific heat of the samples were measured. Nanofluids prepared by means of a dry mixing method presented the lowest viscosity, trimodal particle size distribution and lack of stability. The commonly used dissolution method coupled with oven drying in a petri dish as well as the ball milling method presented non-Newtonian behaviour and intermediate values of particle size and stability. The new spray drying method proposed provided a monomodal particle size distribution with high stability but the highest viscosity and shear thickening behaviour. Results suggest that the four methods evaluated are appropriate for specific heat enhancement (up to 21.1%) but a commitment between stability and viscosity has to be achieved.

Keywords: nanofluid; molten salt; rheology; particle size distribution; specific heat

1. Introduction

The use of renewable energies has become of great importance over the last few years in order to reduce the consumption of fossil fuels and to mitigate Global Warming [1,2]. Concentrated Solar Power (CSP) plants, transforming solar energy into electricity, have the advantage of including a Thermal Energy Storage (TES) system to handle the intermittencies of solar availability and to prevent the gap between energy supply and power demand. The TES material commonly used in CSP plants is the mixture of sodium and potassium nitrates (60-40 wt.%) known as solar salt. In some of the facilities, this material is used as both sensible heat TES and Heat Transfer Fluid (HTF).

Since the first works reported by Shin and Banerjee in 2011 [3,4], in which an abnormal enhancement of the specific heat of molten salts was observed with the addition of nanoparticles, many efforts have been done on the formulation and characterization of molten salt-based nanofluids (colloidal suspensions of particles between 1 and 100 nm) [5-21]. These studies are mainly focused on the influence of the process variables (base fluid, particle size and shape, chemical composition, etc.) and the possible mechanisms behind this abnormal behaviour. It is accepted that the specific heat enhancement depends on the degree of dispersion of the nanoparticles and specific surface available for the interaction between nanoparticles and salt to take place [22, 23].

Less attention has been paid to the modelling of the rheological behaviour of molten salt-based nanofluids [24-28]. In these works, the influence of the type and concentration of nanoparticles, the presence of salt impurities and the measurement equipment on the flow behaviour were studied. Nevertheless, discrepancies about the Newtonian or non-Newtonian behaviour of molten salt-based nanofluids can be found.

For low viscous fluids and very dilute or well dispersed suspensions a Newtonian behaviour is expected. In this case, the mean distance between particles is large compared to the particle radius and particles are able to move freely driven by the Brownian motion. At high volume fractions the particle movement is constricted by the neighbour ones and the hydrodynamic interactions become important. Under these conditions particles agglomerate and nanofluids present shear thinning behaviour [29]. This shear dependent behaviour is due to the clusters, agglomerates, flocs or clusters of flocs that break into primary flocs or individual particles as the shear rate is increased leading to the concept of shear-dependent structure [30]. Moreover, these nanofluids present an apparent yield stress that can be used to analyse the degree of agglomeration.

As both, thermal properties and flow properties depend on the degree of dispersion of the nanoparticles, the production method chosen to disperse the nanoparticles in the base fluid is crucial. Several techniques can be found in the literature being the dissolution method the most widely used technique [5]. In this method the nanoparticles are dispersed in the salt solution and then the water content is removed by evaporation either in a hot plate or an oven with different temperature and evaporation time. Some other methods have been also proposed in which the nanoparticles and the salts are directly mixed up either in solid o molten state with a mortar or mechanical stirrers. Finally, milling in a ball mill or in situ production have also been used. Table 1 summarizes the methods used to prepare molten salt-based nanofluids in the publications mentioned above.

Table 1. Summary of production methods of molten salt-based nanofluids

Method	**References**
Dissolution method + hot plate drying	[6], [7], [8], [10], [16], [22], [25], [27]
Dissolution method + oven/furnace drying	[15], [19], [23], [28], [21]
Magnetical stirring in molten state	[9]
Mechanical stirring in molten state	[17], [18]
Static mixing in molten state in a furnace	[11]
Twin screw micro-compounder mixing in molten state	[14]
In-situ production	[12], [13]
Dry milling in a ball mill	[26]
Dry mixing	[20], [21]

The final particle or cluster size of the nanoparticles dispersed in the molten salt is needed in order to evaluate the efficiency of the production method and its influence on the thermophysical properties. Selvakumar and Dhinkaran [31] developed a model to predict the volume fraction of clusters present in a nanofluid from the particle size distribution measurement. This effective volume fraction can be used to model the rheological behaviour. However, due to the high melting temperature of the solar salt, no direct measurements of particle size distribution were possible until now with the commercial devices available. Recently, authors have developed a new experimental set-up composed of an external, portable dynamic light scattering system coupled with a high temperature cuvette compatible with molten salts to measure for the first time the particle size distribution of the nanoparticles suspended at high temperature conditions [32].

In this work, solar salt-based nanofluids containing a 1 wt.% of silica nanoparticles were produced by four different methods: dry mixing in a mortar, dissolution method and oven drying, dissolution method and spray drying and wet milling in a ball mill

with acetone. The particle size distribution and the stability of the nanofluids were measured in order to analyse the influence of the production method. The rheological behaviour and the specific heat capacity were also measured and the results revealed differences due to the different cluster structure provided by the evaluated methods.

2. Materials and methods

2.1 Materials

Solar salt is the name given to the mixture of $NaNO_3$ and KNO_3 commonly used in the solar thermal industry whose melting temperature is 223ºC. $NaNO_3$ (Analytical grade ACS, Labkem) and KNO_3 (Extra pure, Scharlau) were mixed in a 60:40 wt.% proportion.

The silica nanoparticles used for the nanofluids were obtained from a commercial suspension (Ludox SM-30, 30 wt.% suspension in water, Sigma Aldrich). These are particles well dispersed in water with a narrow size distribution (mean particle size of 25 nm) and a specific surface of 320-400 m^2/g.

2.2 Production methods

Solar salt-based nanofluids with 1 wt.% of silica nanoparticles were prepared by means of four different methods as follows:

(S1) Dry mixing in a mortar: the corresponding amount of Ludox suspension was dropped on the dry solar salt and the mixture was hand mixed. To remove the small amount of water coming from the silica suspension the sample was dried overnight (15 h) in an oven at 100ºC. The dry nanocomposite was finally ground in a porcelain mortar.

(S2) Dissolution method and oven drying: this is the most commonly used method to prepare salt-based nanofluids. First, the solar salt was dissolved in water (1g

salt/10ml water) and then the Ludox suspension containing the nanoparticles was added and dispersed by means of an ultrasound probe (Sonopuls HD2200, Bandelin, HF-output of 200 W and HF-frequency of 20 kHz) for 1 minute at 100% of power input. Samples of 25 ml were distributed in petri dishes and dried overnight (15 h) in an oven at 100ºC. Finally, the powder was recovered from the petri dishes and homogenised with the help of a porcelain mortar.

(S3) Dissolution method and spray drying: in this method the dispersion was carried out in the same manner as in method (S2). The solar salt was dissolved in water (1g salt/10ml water) and the Ludox suspension containing the nanoparticles was dispersed by means of the ultrasound probe. Two litres of nanofluid were prepared and sonication was applied for 1 minute at 100% power input to aliquots of 200 ml. The drying stage was performed by spray drying in a pilot-scale spray dryer Mobile Minor (GEA Niro, Denmark) following the scheme in Figure 1. The suspension was atomized in single droplets using a two-fluid nozzle (1.5 mm of inner diameter) located in the cone of the drying chamber, spraying upwards. Atomization is created by compressed air at a pressure of 1 bar. The drying air is introduced at 380ºC in the centre of the chamber roof, being the outlet temperature of 100-110ºC. Under these conditions, the wet bulb temperature at which the droplet is submitted is 62.7ºC. The spray dried powder is collected with the help of a cyclone. This technique provides a faster drying (a few seconds), allows the production of higher amounts of solar salt containing dispersed nanoparticles and can be scaled up to industrial applications. Although the drying of the droplet is very fast, the whole time needed to spray dry 2 litres of sample can take up to 2 hours. In the meantime the aqueous nanofluid was periodically stirred but no continuous sonication was applied.

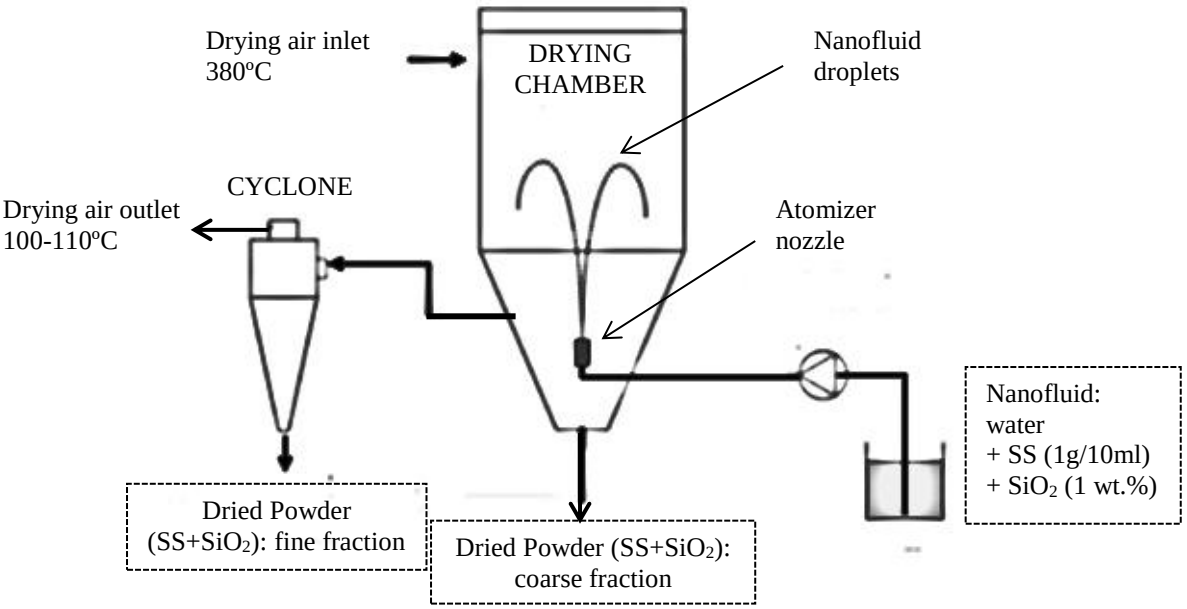

Figure 1. Spray drying set-up.

(S4) Ball milling: to avoid the contact with water, ball milling in acetone was tested. Milling was carried out in a Pulverisette ball mill (Fritsch GmbH) at 400 rpm for 30 min. An agate milling jar was used with agate balls: 32.7 g of balls of 2 cm of diameter and 14.2 g of balls of 1.5 cm of diameter. Solar salt and Ludox in the corresponding weight were mixed with acetone (1g salt/10 ml acetone) in the milling jar. The sample was then dried overnight (15 h) in the oven. To compare the results with the previous methods two drying temperatures were tested: 60ºC (S4_60) and 100ºC (S4_100).

After the production of the solar salt containing dispersed nanoparticles by means of the four methods mentioned above, the powder was melted at 300ºC, stirred for 10 minutes at 1000 rpm using a mechanical stirrer (Eurostar digital, IKA Labotechnik) and then immediately cooled down in the form of pellets.

Table 2 summarizes the experimental conditions of the methods under research.

Table 2. Summary of experimental conditions for nanofluid production methods.

Method	Materials	Nanoparticle dispersion	Liquid removal	Production time for 50 g
S1) Dry mixing	Solar Salt Ludox	Mortar	Oven at 100ºC	<20 h
S2) Dissolution and oven drying	Solar Salt Ludox Water	Ultrasound probe	Oven at 100ºC	< 24 h
S3) Dissolution and spray drying	Solar Salt Ludox Water	Ultrasound probe	Spray drier, droplet temperature 62.7ºC	<5 h
S4) Ball milling	Solar Salt Ludox Acetone	Ball mill	Oven at 60ºC	< 20 h
			Oven at 100ºC	

3. Experimental techniques

3.1 Transmission Electron Microscopy, TEM

The size and shape of the primary particles dispersed in Ludox was observed by means of a Transmission Electron Microscope JEOL 2100 operating at an accelerating voltage of 200 kV. A small amount of the sample was dropped on a copper grid and then was slightly heated to remove the liquid. To prevent agglomeration of particles during the drying of the sample, a very dilute sample was used.

3.2 Rheometry

The viscosity of the nanofluids, η, was obtained by conducting tests under steady state conditions using a Discovery HR-1 rheometer (TA Instruments). A system composed of two parallel plates (40 mm of diameter and 1 mm gap) inside an environmental test chamber was used to measure viscosity at 275ºC. The samples were submitted to the following procedure: (1) a conditioning stage at 275ºC for 30 min, (2) a peak hold stage, in which the samples were submitted to a constant shear rate of 200 s^{-1} for 30 s to ensure similar starting conditions for all the nanofluids, (3) a flow sweep from 1 s^{-1} to the

maximum shear rate and (4) a flow sweep from that maximum to 1 s^{-1}. Both shear rate and time dependant behaviour were evaluated with this procedure.

Torque and axial force values were checked for each test. The minimum shear rate was determined so the torque value was higher than 0.1 μN·m. For lower values the viscosity is affected by the surface tension of the molten salts and the results are not reliable. The maximum shear rate is the one in which the axial force starts to decrease due to turbulent effects in the sample that lead to an apparent increase in the viscosity. The maximum shear rate is 300 s^{-1} for low viscous samples while reaches 1000 s^{-1} for the most viscous sample.

3.3 Dynamic Light Scattering, DLS

In order to measure the particle size, d_P, distribution and stability of molten salt-based nanofluids at high temperature conditions a new system previously developed by the authors was used. A dynamic light scattering (DLS) VASCO FLEX particle size analyser (Cordouan Technologies) consisting of an external laser head that contains the light emitter and receiver was used (65 mW-658 nm fibre pigtailed laser). This device can measure diameters ranging from 0.5 nm to 10 μm. Intensity particle size distributions are obtained in which Y axis is the percentage of light scattered by the particles. The light registered corresponds to backscattering with an angle of 170º. In order to heat up and control the temperature of the samples, a high temperature cuvette was designed. It consists of a cylindrical stainless steel cuvette with two fused quartz windows on the sides with a 20 ml sample volume. A heating ring is installed around the cuvette and two K-thermocouples are used to control the temperature on the wall of the cuvette and inside the fluid. The working temperature of the system was set at 275ºC in order to do not damage the windows (maximum working temperature 300ºC). A more detailed scheme of this experimental set-up can be found in [32].

Initially the pellets were introduced in the cuvette and heated to melt the sample. After complete melting, the fluid was mechanically stirred at 1000 rpm for 2 minutes to ensure homogeneous conditions. Measurements of particle size distributions in static condition were taken every 30 minutes at the beginning and then every 1 hour for 4 hours. The sample was finally redispersed by mechanical stirring at 1000 rpm for 2 minutes to check if the initial particle size was recovered.

3.4 Differential Scanning Calorimetry, DSC

The specific heat of the nanofluids, c_P, was measured by means of differential scanning calorimetry (DSC) tests using a DSC2 calorimeter (Mettler Toledo). The method used was the areas method, which has been checked to provide better results than the dynamic or isostep methods [33]. In this method, a standard sapphire and the sample were submitted to consecutive isothermal segments with a 1 ºC step and no heating stages amid. The DSC signal provided a peak, whose area was used to calculate the specific heat. A 1 ºC temperature step was applied at 400 ℃, with 5 minute isotherms before and after the step. A sample of around 20 mg was analysed in a 40 μl aluminium crucible. Tests were carried out at a constant 25 mL/min N_2 flow rate. To ensure repeatability at least three samples were prepared and two cycles were run for each one in order to obtain a mean value. The experimental error of the mean value was statistically obtained at a 95% of confidence level, with a maximum error of 5.02% and a mean error of 2.39%.

Phase change performance of the samples was also evaluated by means of DSC. A sample of around 20 mg was analysed in a 40 μl aluminium crucible. A thermal cycle from 180 ºC to 280 ºC was performed under nitrogen atmosphere (25 mL/min N_2 flow rate), with 10 K/min heating and cooling rates and 5 min isotherms at the maximum and minimum temperatures.

3.5 Thermogravimetric analysis, TGA

The thermal stability of the samples and the decomposition temperature was evaluated by means of Thermogravimetric Analysis (TGA) using a TGA/SDTA851e (Mettler Toledo). Samples were submitted to a 5 minute isotherm followed by a heating step from 25 ºC to 900 ºC at 10 K/min under N_2 atmosphere in an alumina crucible.

4. Results and discussion

4.1 Viscosity and rheological behaviour

The dynamic viscosity and the rheological behaviour of the nanofluids were measured following the procedure previously explained. The flow curves obtained for the samples tested are shown in Figure 2. Regarding the shear dependent behaviour it can be observed that the pure solar salt as well as the sample prepared by dry mixing (S1) present a Newtonian behaviour with the lower viscosity values. The sample prepared by the dissolution method (S2) coupled with oven drying present shear thinning behaviour thus indicating the presence of agglomerates that break down to smaller ones due to the application of high shear rates [30]. For the samples prepared by ball milling (S4_60 and S4_100) and the dissolution method coupled with spray drying (S3), an abnormal behaviour is observed. A first shear thinning region can be initially observed followed by a shear thickening region and a second shear thinning region. This shear thickening behaviour is more noticeable as the viscosity of the samples increases and is reached at lower values of shear rate. For the S3 the first shear thinning region can be initially observed up to 25 s^{-1} followed by a shear thickening region up to 65 s^{-1} and a second shear thinning region. This behaviour was first observed in the literature for ionic liquids in 2009 [34] and has been recently reported for molten salt-based nanofluids [35]. This behaviour is common in concentrated suspensions of ionic liquids in which, due to the interparticle forces acting on the particle surface, agglomeration and jamming

take place when particles get into contact because of the fluid flow at a sufficient shear rate. When a threshold shear rate is achieved these agglomerates break down into smalls ones leading to the second shear region.

Regarding the time dependant behaviour, only the nanofluid prepared by the dissolution method coupled with spray drying (S3) presents rheopectic behaviour for shear rates lower than 65 s^{-1} caused by the shear thickening behaviour. Reversible time effects have been reported in some materials including colloidal suspensions, in which the viscosity increases with time at low shear rates after shearing at high shear rates [36]. This sample was submitted to a third flow sweep from 1 s^{-1} to 1000 s^{-1} to check the reversibility of the process and the recovery of the initial particle structure as can be observed.

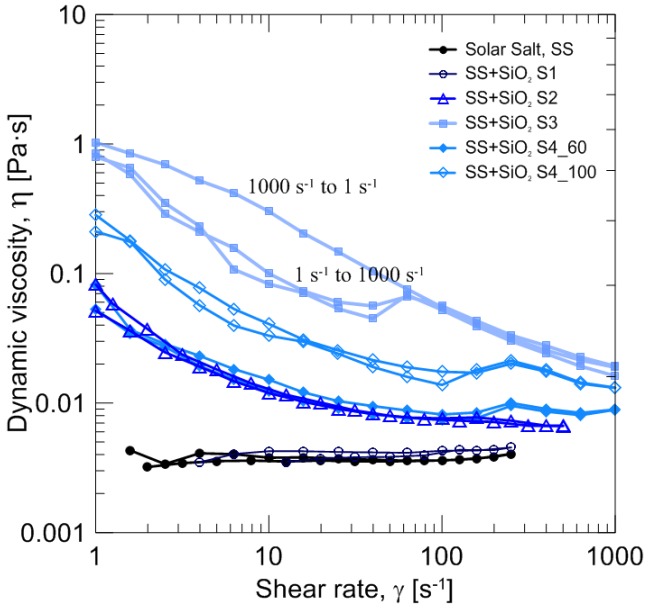

(a)

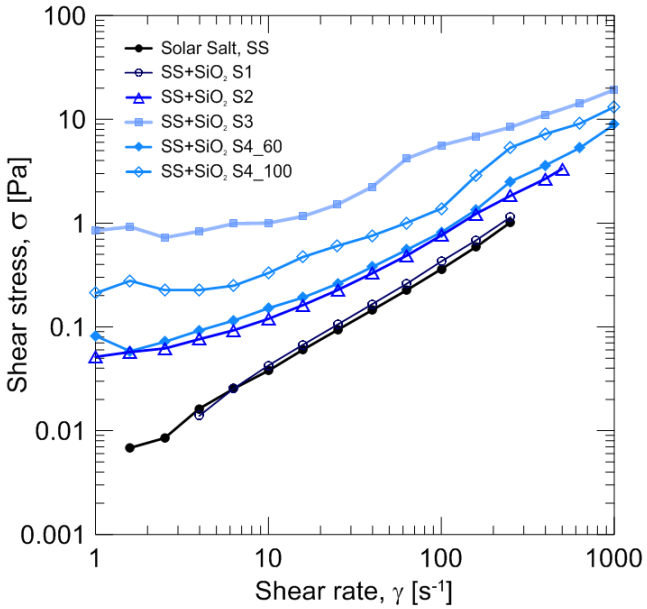

(b)

Figure 2. Solar salt-based nanofluids (a) flow curve and (b) shear stress vs. shear rate at 275°C.

As the nanofluid composition is the same for all the samples, the differences found in the rheological behaviour are expected to be linked to the different agglomeration states achieved during the production method. Two of the parameters most widely used to

analyse the degree of agglomeration are the extrapolated yield stress, σ_Y, and the plastic viscosity, η_P, [37]. These parameters can be obtained by fitting the shear stress/shear rate values in the Newtonian plateau to the Bingham model:

$$\sigma = \sigma_Y + \eta_P \cdot \gamma \quad (1)$$

where σ is the shear stress applied and γ is the shear rate generated and shown in Figure 2b.

Results are shown in Table 3. For the two samples presenting Newtonian behaviour (pure Solar Salt and the nanofluid obtained by S1 method), no yield stress is obtained and the plastic viscosity corresponds to the dynamic viscosity of the fluid, independent of the shear rate. For the non-Newtonian nanofluids the extrapolated yield stress is obtained being higher for the sample with the highest viscosity. These results confirm the differences in the agglomeration state when the nanofluids are produced by different methods.

Table 3. Yield stress and plastic viscosity.

Sample	σ_Y **[Pa]**	$\eta_P \cdot 10^3$ **[Pa·s]**	R^2
Solar Salt SS	-	3.90	0.998
SS+SiO_2 S1	-	4.44	0.999
SS+SiO_2 S2	0.045	7.21	0.997
SS+SiO_2 S3	1.695	19.07	0.964
SS+SiO_2 S4_60	0.049	8.02	0.998
SS+SiO2 S4_100	0.202	12.14	0.994

In order to obtain the viscosity enhancement caused by the dispersion of the nanoparticles by means of the different methods, the viscosity of the nanofluids at the maximum shear rate (Newtonian plateau) was used for the non-Newtonian nanofluids. In Table 4 it can be observed that for the pure solar salt the value obtained is in good agreement with the theoretical one in the literature for 275ºC ($4.25 \cdot 10^{-3}$ Pa·s) [38]. In all

cases the viscosity increases with the addition of nanoparticles, as expected. However, the increase strongly depends on the production method. The dry mixing method (S1) provides a Newtonian behaviour with the lowest increase while the dissolution method coupled with spray drying (S3) leads to non-Newtonian, rheopectic behaviour with the highest increase. In the ball milling method it can be observed how the increase in the drying temperature from 60ºC to 100ºC reduces the drying time and leads to a different microstructure of the nanoparticles with a higher viscosity.

Table 4. Viscosity increase at the maximum shear rate.

Sample	$\eta \cdot 10^3$ **[Pa·s]**	**Viscosity increase [%]**
Solar Salt, SS	3.90	-
SS+SiO_2 S1	4.44	13.7
SS+SiO_2 S2	6.68	71.2
SS+SiO_2 S3	19.25	393.5
SS+SiO_2 S4_60	8.92	128.8
SS+SiO2 S4_100	13.16	237.4

4.2 Particle size distribution and colloidal stability

As has been mentioned before the differences found in the viscosity of the samples are expected to depend on the particle size and agglomeration. At low shear rates this viscosity can be related to the particle/cluster size measured in static conditions. Figure 3 show the particle size distribution of the primary nanoparticles obtained by image processing of over 1000 particles observed by TEM. A micrograph of the nanoparticles is shown and a mean particle diameter of 25 nm is obtained.

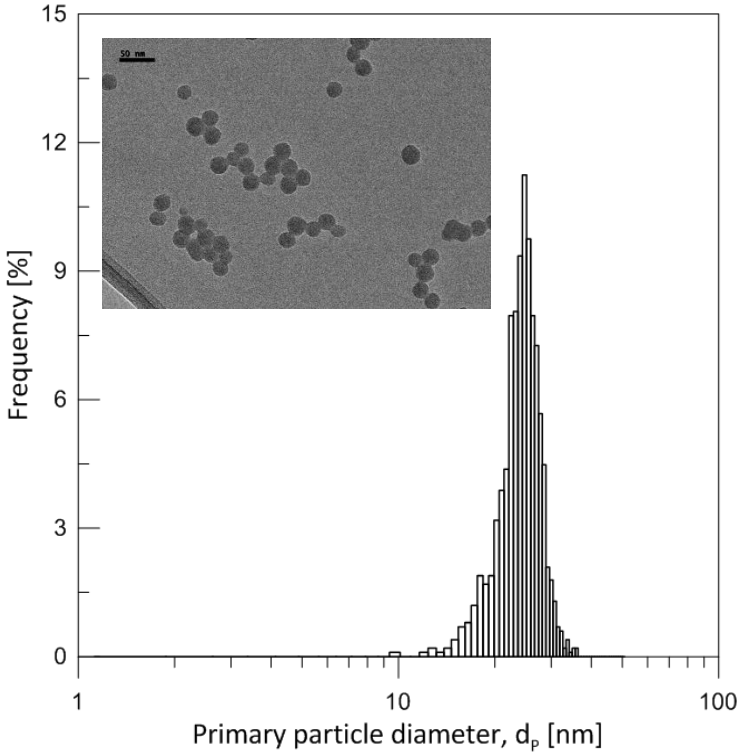

Figure 3. Primary particle size distribution and TEM micrograph.

In spite of the good dispersion of the primary nanoparticles, they agglomerate when introduced in the molten salt. Figure 4 shows the initial particle size distribution measured for the nanofluids tested. It can be observed that the only sample presenting a monomodal distribution is the sample S3 (spray drying method). The other four samples present multimodal distributions with small particles at around 100 nm and agglomerates bigger in the micrometrical size range. These differences found in the initial size confirms that the cluster structure of the sample produced by means of spray drying (S3) is completely different from the other samples which can be related to the different rheological behaviour and the highest viscosity.

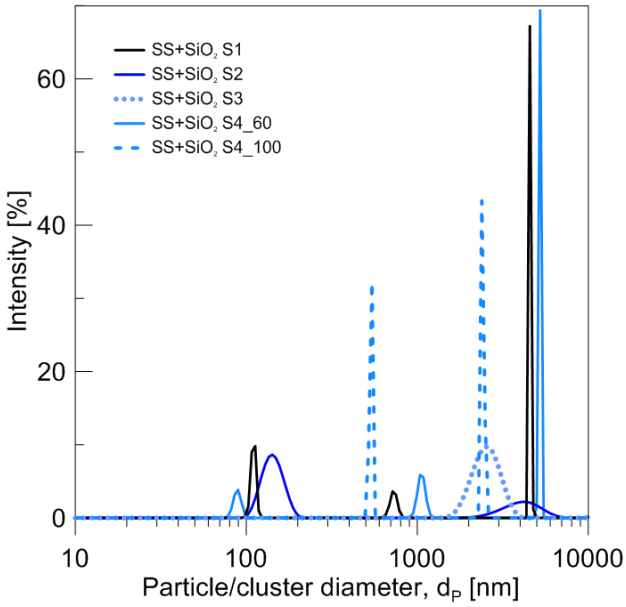

Figure 4. Initial particle/cluster size distribution.

In order to evaluate the colloidal stability of the samples, the evolution of the particle/cluster size distribution with time was measured for 4h in static conditions and after redispersion. Initial size, agglomeration after 4h in static conditions and size after redispersion of the particles are plotted in Figure 5. It can be observed that the samples S1, S2 and S4_60 initially show a smaller peak around 100 nm and then clusters of bigger sizes, reaching up to a few thousand nanometres. Samples S1, S2, S4_60 and S4_100 also present a general displacement of the peaks after 4 hours, showing bigger clusters that reach up to 10000 nm in some cases, the maximum size that the equipment can register. The behaviour after redispersion is different for every sample. In S1, the redispersion does not change much compared to the state after 4 hours, and a peak at the limit of 10000 nm still appears. A similar behaviour is observed for S2, where a peak of bigger clusters remain after the redispersion, even though there is also a peak of small particles below 100 nm that indicates that some of the bigger clusters have broken down with redispersion. Sample S4_60 presents an only peak, so redispersion seems to be effective to reduce the cluster sizes to 1000 nm. In sample S4_100 the redispersion is

effective enough to recover the initial the particle size. The behaviour of S3 is completely different to the rest of the studied samples, in line with what has been observed in the rheology tests. This sample shows a big peak between 2000 and 3000 nm in every stage studied, and also presents bigger clusters around 10000 nm after 4 hours, that are effectively recovered after redispersion.

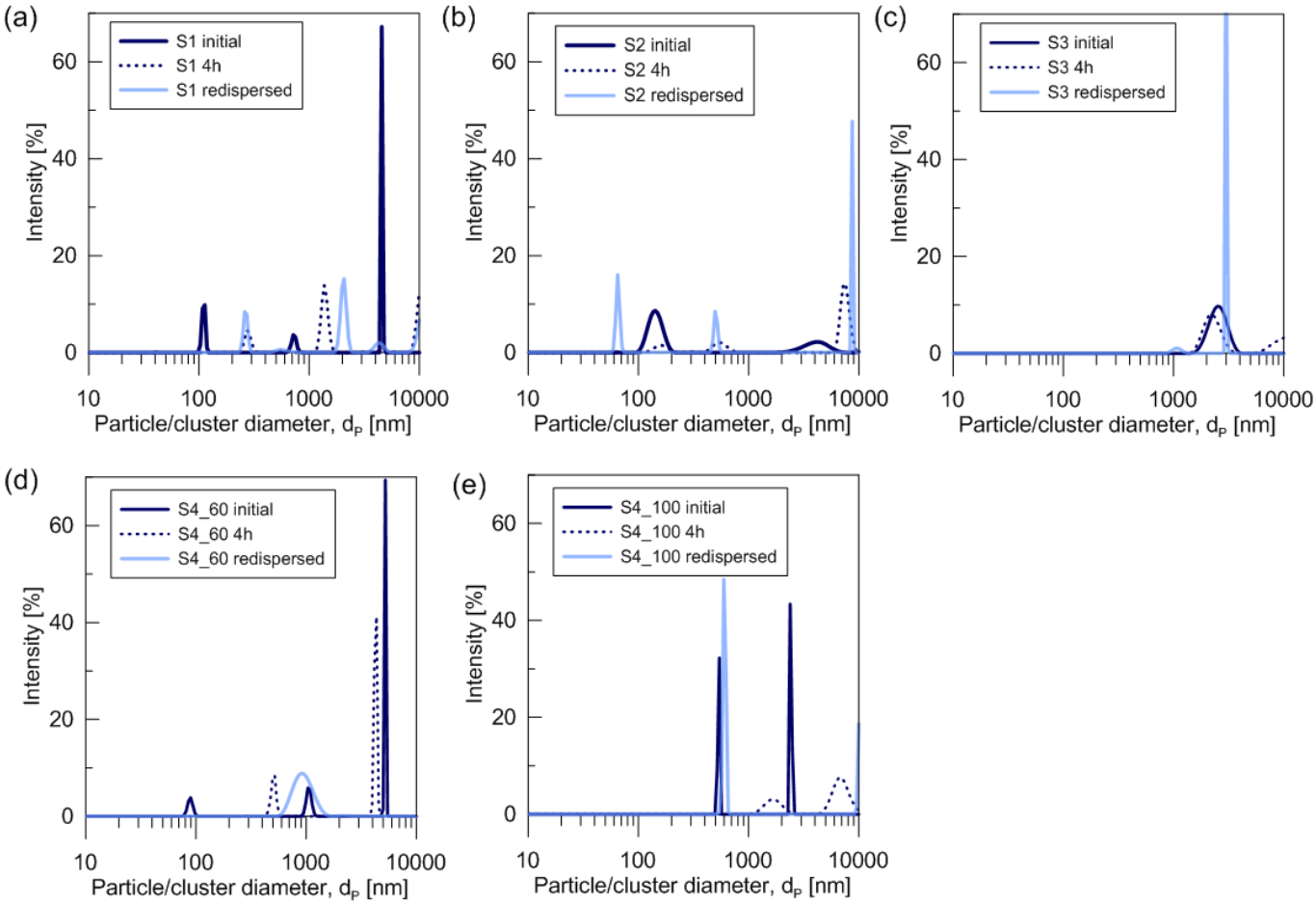

Figure 5. Particle/cluster size distribution: initial, after 4h and redispersed for (a) S1, (b) S2, (c) S3, (d) S4_60 and (e) S4_100.

Figure 6 shows the evolution of the main peaks of the size distribution through time. As the size distributions were not monomodal and a mean particle size cannot be used, the size of the peaks obtained at any measured time was plotted. Bigger bubbles correspond to higher intensity peaks detected, namely, a higher amount of light scattered by the

particles. As the intensity of the scattering is proportional to the sixth power of the diameter according to Rayleigh's approximation, small particles scatter less light than big particles. Therefore small particles presenting a high intensity indicates a higher amount of clusters of that size. It is observed that for the sample S1 the distribution remains trimodal with time and the bigger clusters agglomerate up to diameters close to 10 μm while the smaller ones remain rather constant. Samples S2, S4_60 and S4_100, are bimodal most of the time and the change in the bigger agglomerates is observed in the last hour recorded. In the samples S2 and S4_100 an increase is observed while in the sample S4_60 a decrease takes place due to settlement of clusters, both behaviours meaning a lack of stability. The sample S3 is the only one presenting a rather monomodal and stable behaviour over time. In this case, the high viscosity of the nanofluid helps to keep particles in suspension avoiding their settlement. It can be concluded that faster dryings (S2 and S4_100) lead to smaller initial clusters as the nanoparticle do not have so much time to agglomerate than in the other ones.

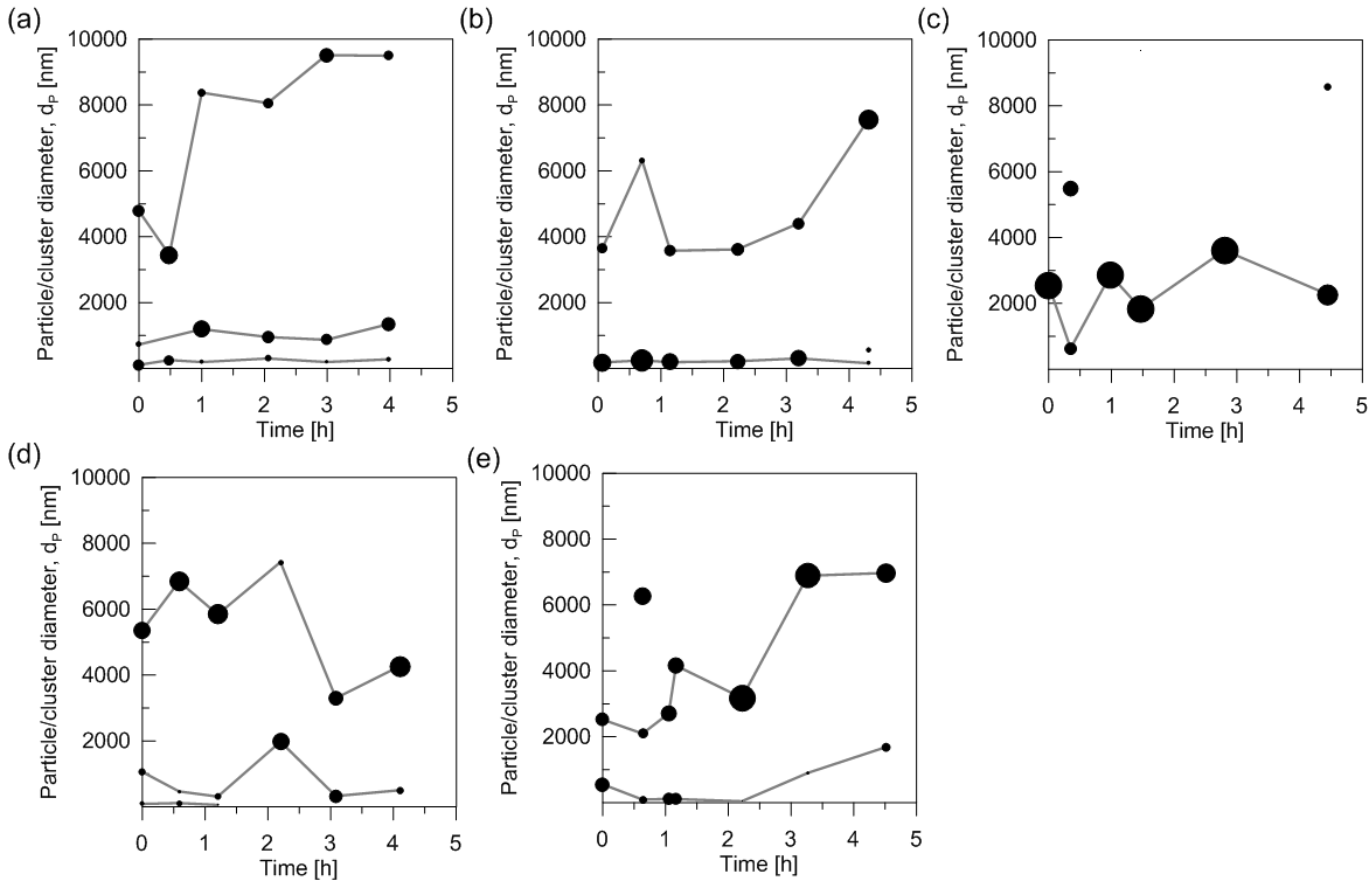

Figure 6. Evolution of particle size with time for (a) S1, (b) S2, (c) S3, (d) S4_60 and (e) S4_100.

The stability of the nanofluids can be theoretically predicted through the forces acting in the nanofluid. Among them, Stokes sedimentation due to gravity and diffusivity due to Brownian motion can be used to calculate the colloidal stability limit of a suspension [39]. The colloidal stability limit is the critical size of a particle or particles cluster for which the displacement due to the Brownian motion equals the one due to the Stokes sedimentation. Thus, if they have bigger dimensions than the colloidal limit the Stokes sedimentation becomes predominant and the particles will settle being the nanofluid not stable through time. The diffusion of a particle due to Brownian motion can be calculated through the following equation:

$$X = \left[t \frac{2 \cdot k \cdot T}{3 \cdot \pi \cdot \eta \cdot d_P} \right]^{1/2} \quad (2)$$

where t is time in seconds, k is Boltzmann's constant, T is temperature in Kelvin, η is the dynamic viscosity of the nanofluid, and d_P is the particle diameter.

On the other hand, the displacement due to the Stokes sedimentation can be calculated as shown in the following equation:

$$X = \frac{d_P^2 \cdot (\rho_P - \rho_{nf}) \cdot g \cdot t}{18 \cdot \eta} \quad (3)$$

where ρ_p is the density of the particle, ρ_{nf} is the density of the nanofluid and g is the acceleration due to gravity.

The intersection between both parameters determines the colloidal limit for a particular nanofluid, as it can be observed in Figure 7. All the calculations have been made for a time of 300 s and the viscosity of the samples at the lowest shear rate has been used. Results can be linked with the evolution of the particle size previously obtained (Figure 6). For sample S1 the colloidal limit is found at ca. 1000 nm which is in good agreement with results shown in Figure 6a: particles and agglomerates of lower size remain stable while the big ones continue to agglomerate being the least stable nanofluid. For the samples S2 and S4_60 the colloidal limit is found at ca. 1800 nm presenting both bimodal particle size distributions with stable agglomerates of diameter lower than the limit and bigger ones which agglomerate and settle (Figures 6b and 6d). Regarding the drying temperature for samples S4_60 and S4_100, the latter presents a higher viscosity and colloidal limit (ca. 2250 nm). Although the initial particle size is smaller, the same behaviour can be observed: small clusters are stable while the bigger ones are very close to the stability limit and agglomerate. Finally, sample S3 present a colloidal limit at ca. 3000 nm. In this case all the agglomerates initially present in the nanofluid present a diameter smaller than the limit and therefore the nanofluid is expected to be stable.

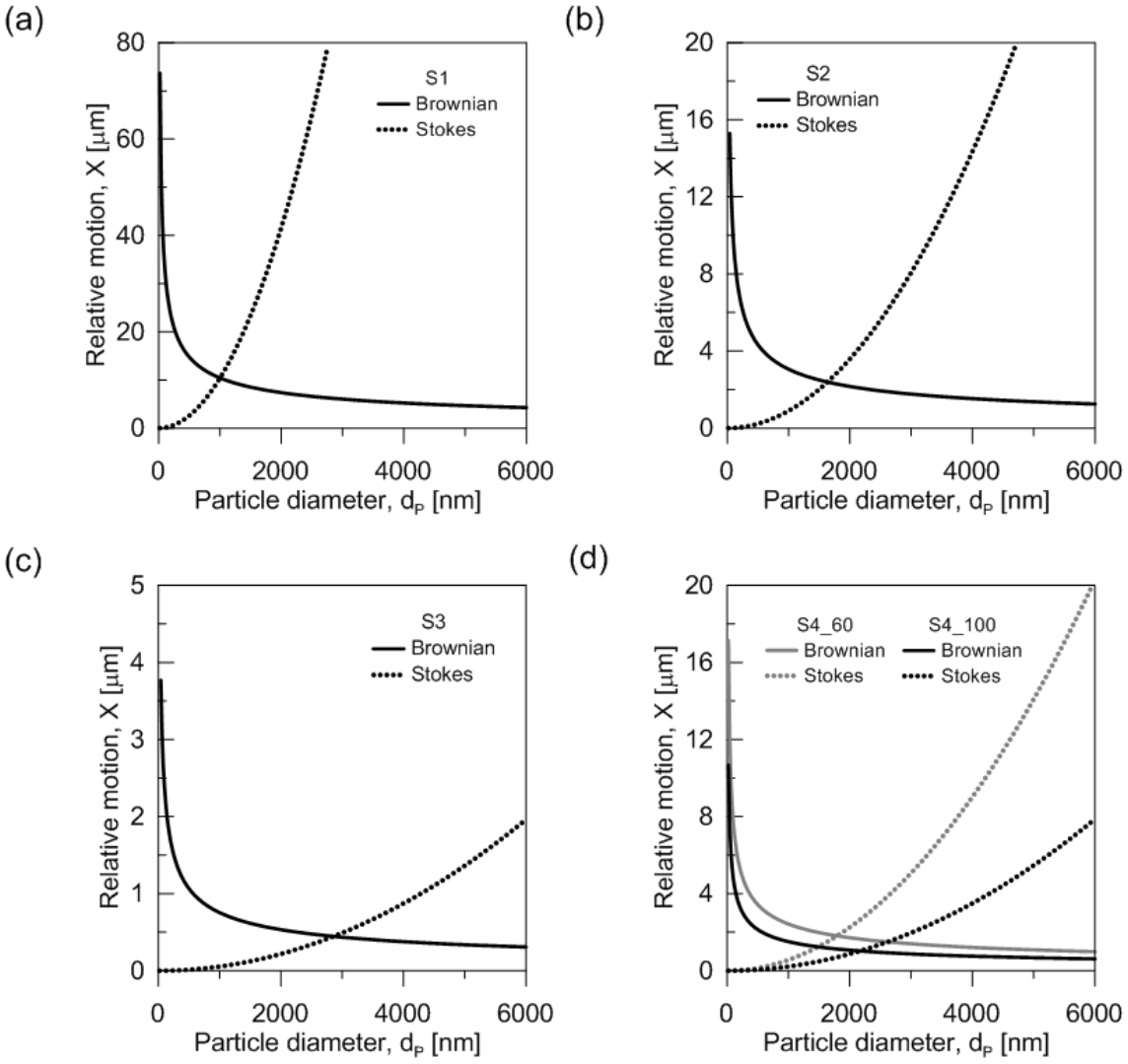

Figure 7. Colloidal stability limit for samples (a) S1, (b) S2, (c) S3 and (d) S4.

4.3 Specific heat capacity

Table 5 shows the results obtained for the specific heat at 400ºC for the samples under research. It can be observed that for the pure solar salt the value obtained is in good agreement with the theoretical one in the literature (1.511 J/gK) [38]. Regardless of the differences observed in the particle size, the samples with the highest enhancement are the ones that were processed at 100ºC overnight in aqueous medium, i.e. S1 and S2. Samples S3 (spray drying) and S4_60 (ball milling) were submitted to lower temperatures around 60ºC and the enhancement is lower. Comparing samples S1, S2

and S4_100 it can be observed that the specific heat is lower for the samples processed in acetone in which the drying is faster. From the samples S4_60 and S4_100 the influence of the temperature on a same method can be evaluated and it is concluded that the specific heat increases with temperature. The lowest value obtained corresponds to the spray dried sample in which not only the temperature is low but also the residence time is reduced so the material is not able to heat up to the maximum drying air temperature.

Although there is still controversy about the possible mechanisms behind the specific heat enhancement, these results are in agreement with one of the most widely accepted mechanism for the abnormal specific heat enhancement of ionic liquids [3, 4, 23, 40]. The mechanism takes into account the formation of an interfacial structure resulting from the discrete layering of ions at the solid surface due to nanoparticle-salt interactions. Therefore, the experimental conditions that could modify these possible interactions, such as the drying temperature and time, can also influence the specific heat enhancement.

In conclusion, the method used to prepare the molten salt-based nanofluids is crucial being samples S1 and S2 the best candidates from the point of view of thermal energy storage capability.

Table 5. Specific heat increase at 400ºC.

Sample	**Specific heat, c_P [J/gK]**	**Specific heat increase [%]**
Solar Salt SS	1.496	-
SS+SiO_2 S1	1.812	21.1
SS+SiO_2 S2	1.800	20.3
SS+SiO_2 S3	1.638	9.5
SS+SiO_2 S4_60	1.655	10.6
SS+SiO2 S4_100	1.733	15.82

Finally, the possible relationship between the viscosity and specific heat increases with the particle size was evaluated. Figure 8 shows the evolution of the property increase with the size of the smallest peak initially present in the nanofluid. As a general trend, it can be observed that the presence of the bigger clusters leads to higher viscosities and lower specific heat values. However, an exemption can be found for smaller sizes thus meaning that not only the particle size but also other parameters influence the specific heat enhancement as mentioned before.

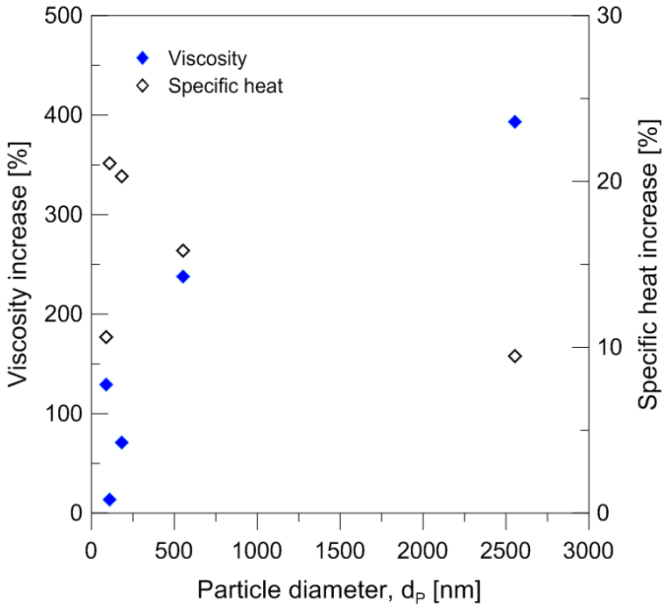

Figure 8. Evolution of viscosity and specific heat increases with particle size.

4.4 Thermal and chemical stability

The thermal and chemical stability of the molten salt-based nanofluids was evaluated by means of TGA and DSC tests as shown in Figure 9a and Figure 9b respectively. The weight loss for the silica nanoparticles obtained after drying of the Ludox commercial nanofluid at 100 ºC in the oven was also tested. A low weight loss is observed in the nanoparticles probably due to presence of the additives used to stabilize the water-based nanofluid. However, the influence of these additives on the thermal properties of the

molten salt-based nanofluids is negligible as can be observed in the TGA curves. No significant differences between the nanofluids and the pure solar salt were found for the weight loss and the decomposition temperature. The same conclusion can be gathered from the DSC curves in which no significant differences were observed for the phase change temperatures and enthalpies of the nanofluids with respect to the pure solar salt.

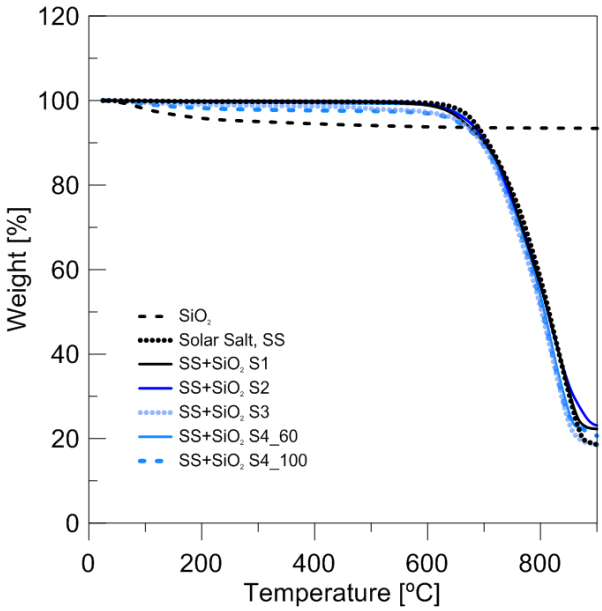

(a)

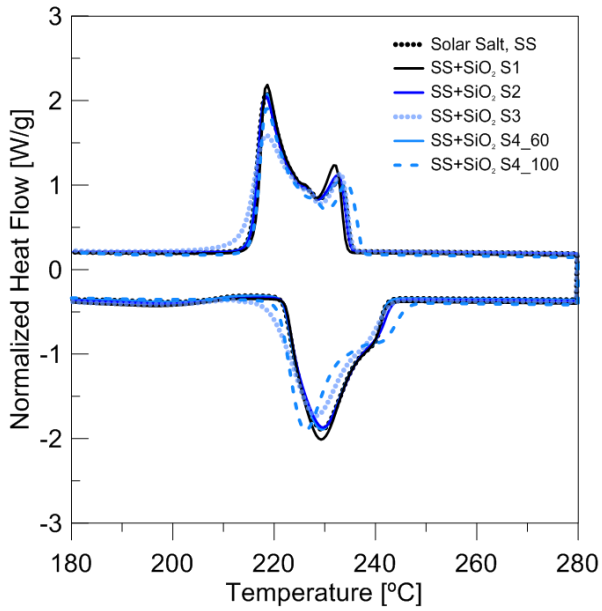

(b)

Figure 9. (a) TGA curves and (b) DSC curves for the samples.

5. Conclusions

Solar salt-based nanofluids have been produced by means of four different methods involving wet routes. In addition to the methods previously used in the literature (dry mixing, oven drying and ball milling), spray drying in a pilot-scale spray dryer was used as an example of industrial scale process. The particle size distribution of the nanoparticles suspended in the molten salt at 275 ºC was measured by a new DLS system and the degree of agglomeration and stability of the samples were evaluated. Rheological behaviour and specific heat of the samples, both properties depending on the particle size and clustering, were measured to analyse the influence of the production method.

- The dry mixing method (S1) provided the lowest viscosity increase and Newtonian behaviour. However, in this sample a trimodal particle size distribution was observed and the nanoparticles agglomerate with time, meaning that the nanofluid is not stable.
- The dissolution method coupled with oven drying (S2) and the ball milling method (S4) provided similar shear thinning behaviour with higher viscosity increments. Although the particle size distributions are mainly bimodal, the samples start to lose stability after 3 h in static conditions.
- The dissolution method coupled with spray drying (S3) provided the highest viscosity increment with shear thinning and shear thickening regions leading also to rheopectic behaviour. This sample was the only one presenting a monomodal distribution and good stability over time probably caused by the high viscosity.
- The colloidal stability limit obtained from the Brownian motion and the Stokes settlement calculations depends mainly on the nanofluid viscosity. The results

are in good agreement with the evolution of the particle size distribution with time and can be used to predict the colloidal stability.

- Regarding the specific heat, all the samples provided an enhancement suitable for thermal energy storage applications. This enhancement is mainly dependent on the agglomeration state and the drying temperature and time. For samples with similar cluster size and viscosity (S2 and S4_60), the higher the drying temperature the higher the specific heat achieved. Comparing the same method (S4), also the highest drying temperature provided a higher specific heat enhancement although not the highest due to the fast drying. In general, the optimal conditions to increase the specific heat include slow drying at high temperature.

In conclusion, the production method needs to be controlled in order to achieve an appropriate degree of dispersion of the nanoparticles. A commitment between stability and viscosity has to be achieved as the most stable nanofluid is also the most viscous. Finally, the temperature and time at which the nanoparticles are submitted during the production process can be optimized to promote nanoparticle salt interactions and to improve the thermal energy storage capacity of the nanofluids in combination with higher production rates required for large-scale production.

Acknowledgements

The authors want to thank the financial support from Ministerio de Economía y Competitividad (MINECO) (project ENE2016-77694-R) and Universitat Jaume I (project UJI-B2016-47). Nuria Navarrete thanks Universitat Jaume I for a pre-doctoral fellowship (Ref. PREDOC/2016/28) that made possible the research carried out in this work. ***This***

work was partially funded by the Agencia Estatal de Investigación (AEI) of the Ministerio de Ciencia, Innovación y Universidades (RED2018-102431-T). Authors thank Servicios Centrales de Instrumentación Científica (SCIC) of Universitat Jaume I for the use of TEM (Maria del Carmen Peiró) and DSC (Cristina Zahonero) and Instituto de Tecnología Cerámica of Universitat Jaume I for the use of TGA. This work has been developed by participants of the COST Action CA15119 Overcoming Barriers to Nanofluids Market Uptake (NANOUPTAKE).

References

1. Alva, G., Lin, Y., Fang, G. An overview of thermal energy storage systems. Energy 144, 341-378 (2018).
2. Mahian, O., Kianifar, A., Kalogirou, S.A., Pop, I., Wongwises, S. A review of the applications of nanofluids in solar energy. International Journal of Heat and Mass Transfer 57, 582–594 (2013).
3. Shin, D., Banerjee, D. Experimental Investigation of Molten Salt Nanofluid for Solar Thermal Energy Application. 8th Thermal Engineering Joint Conference AJTEC (2011).
4. Shin, D., Banerjee, D. Enhancement of Specific Heat Capacity of High-Temperature Silica-Nanofluids Synthesized in Alkali Chloride Salt Eutectics for Solar Thermal-Energy Storage Applications. International Journal of Heat and Mass Transfer 54, 1064-1070 (2011).
5. Mondragon, R., Navarrete, N., Gimeno-Furio, A., Hernandez, L., Cabedo, L., Julia, J.E. Advances in New Heat Transfer Fluids From Numerical to Experimental Techniques. Chapter 11- New High-Temperature Heat Transfer and Thermal

Storage Molten Salt–Based Nanofluids Preparation, Stabilization, and Characterization. Taylor & Francis Group, LLC. (2017).

6. Shin, D., Banerjee, D. Enhanced Specific Heat Capacity of Nanomaterials Synthesized by Dispersing Silica Nanoparticles in Eutectic Mixtures. Journal of Heat Transfer 135, 32801 (2013).

7. Tiznobaik, H., Shin, D. Enhanced specific heat capacity of high-temperature molten salt-based nanofluids. International Journal of Heat and Mass Transfer 57, 542-548 (2013).

8. Lu, M.C., Huang, C.H., Specific heat capacity of molten salt-based alumina nanofluids. Nanoscale Res Lett. 8, 292–299 (2013).

9. Ho, M.X., Pan, C. Optimal concentration of alumina nanoparticles in molten Hitec salt to maximize its specific heat capacity. Int J Heat Mass Trans70, 174–184 (2014).

10. Jo, B., Banerjee, D., Enhanced specific heat capacity of molten salt-based nanomaterials: Effects of nanoparticle dispersion and solvent material. Acta Materialia 75, 80-91 (2014).

11. Tian, H., Du, L., Huang, C., Wei, X., Wang, W., Ding, J. Enhanced specific heat of chloride salt with Mg particles for high-temperature thermal energy storage. Energy Procedia 105, 4402 – 4407 (2017).

12. Luo, Y., Du, X., Awad, A., Wen, D. Thermal energy storage enhancement of a binary molten salt via in-situ produced nanoparticles. International Journal of Heat and Mass Transfer 104, 658–664 (2017).

13. Lasfargues, M., Stead, G., Amjad, M., Ding, Y., Wen, D. In Situ Production of Copper Oxide Nanoparticles in a Binary Molten Salt for Concentrated Solar Power Plant Applications. Materials 10, 537 (2017).

14. Chieruzzi, M., Cerritelli, G.F., Miliozzi, A., Kenny, J.M., Torre, L. Heat capacity of nanofluids for solar energy storage produced by dispersing oxide nanoparticles in nitrate salt mixture directly at high temperature. Solar Energy Materials and Solar Cells 167, 60–69 (2017).

15. Chieruzzi, M., Miliozzi, A., Crescenzi, T., Kenny, J.M., Torre, L. Synthesis and Characterization of Nanofluids Useful in Concentrated Solar Power Plants Produced by New Mixing Methodologies for Large-Scale Production. Journal of Heat Transfer 140, 042401-1 (2018).

16. Awad, A., Navarro, H., Ding, Y., Wen, D. Thermal-physical properties of nanoparticle-seeded nitrate molten salts. Renewable Energy 120, 275-288 (2018).

17. Chen, X., Wu, Y., Zhang, L., Wang, X., Ma, C. Experimental study on the specific heat and stability of molten salt nanofluids prepared by high-temperature melting. Solar Energy Materials and Solar Cells 176, 42–48 (2018).

18. Chen, X., Wu, Y., Zhang, L., Wang, X., Ma, C. Experimental study on thermophysical properties of molten salt nanofluids prepared by high-temperature melting. Solar Energy Materials and Solar Cells 191, 209–217 (2019).

19. Jiang, A., Palacios, A., Lei, X., Navarro, M.E., Qiao, G., Mura, E., Xu, G., Ding, Y. Novel key parameter for eutectic nitrates based nanofluids selection for concentrating solar power (CSP) systems. Applied Energy 235, 529–542 (2019).

20. Navarrete, N., Mondragon, R., Wen, D., Navarro, M. E., Ding, Y., Julia, J. E. Thermal energy storage of molten salt-based nanofluid containing nano-encapsulated metal alloy phase change materials. Energy 167, 912–920 (2019).

21. Grosu, Y., Nithiyanantham, U., González-Fernández, L. and Faik, A. Preparation and characterization of nanofluids based on molten salts with enhanced thermophysical properties for thermal energy storage at concentrate solar power. In AIP Conference Proceedings (Vol. 2126, No. 1, p. 200021). AIP Publishing (2019).

22. Andreu-Cabedo, P., Mondragon, R., Hernandez, L., Martinez-Cuenca, R., Cabedo, L., Julia, J.E. Increment of specific heat capacity of solar salt with SiO2 nanoparticles. Nanoscale Res Lett. 9, 582–592 (2014).

23. Mondragón, R., Juliá, J.E., Cabedo, L., Navarrete, N. On the relationship between the specific heat enhancement of salt-based nanofluids and the ionic exchange capacity of nanoparticles. Scientific Reports 8, 7532 (2018).

24. Wang, W., Wu, A., Li, B., Sundén, B. A review on molten-salt-based and ionic-liquid-based nanofluids for medium-to-high temperature heat transfer. Journal of Thermal Analysis and Calorimetry 136, 1037–1051 (2019).

25. Jo, B., Banerjee, D., Viscosity measurements of multi-walled carbon nanotubes-based high temperature nanofluids. Materials Letters 122, 212–215 (2014).

26. Lasfargues, M., Cao, H., Qiao, G., Ding, Y. Rheological Analysis of Binary Eutectic Mixture of Sodium and Potassium Nitrate and the Effect of Low Concentration CuO Nanoparticle Addition to Its Viscosity. Materials 8, 5194-5204 (2015).

27. Muñoz-Sánchez, B., Nieto-Maestre, J., Veca, E., Liberatore, R., Sau, S., Navarro, H., Ding, Y., Navarrete, N., Juliá, J.E., Fernández, A.G., García-Romero, A.

Rheology of Solar-Salt based nanofluids for concentrated solar power. Influence of the salt purity, nanoparticle concentration, temperature and rheometer geometry. Solar Energy Materials and Solar Cells 176, 357–373 (2018).

28. Xiao, X., Zhang, G, Ding, Y., Wen, D. Rheological Characteristics of Molten Salt Seeded with Al2O3 Nanopowder and Graphene for Concentrated Solar Power. Energies 12, 467 (2019).

29. Quemada, D., Berli, C. Energy of interaction in colloids and its implication in rheological modeling. Advances in Colloid and Interface Science 98, 51-85 (2002).

30. Quemada, D. Rheological modeling of complex fluids. I. The concept of effective volume fraction revised. EPJ Applied Physics 1, 119-127 (1998).

31. Selvakumar, R.D., Dhinakaran, S. Effective viscosity of nanofluids — A modified Krieger–Dougherty model based on particle size distribution (PSD) analysis. Journal of Molecular Liquids 225, 20–27 (2017).

32. Navarrete, N., Gimeno-Furió, A., Forner-Escrig, J., Juliá, J.E., Mondragón, R. Colloidal stability of molten salt –based nanofluids: Dynamic Light Scattering tests at high temperature conditions. Powder Technology 352, 1–10 (2019).

33. Ferrer, G., Barreneche, C., Solé, A., Martorell, I., Cabeza, L.F., New proposed methodology for specific heat capacity determination of materials for thermal energy storage (TES) by DSC, Journal of Energy Storage, 11, 1-6 (2017).

34. Ueno, K., Imaizumi, S., Hata, K., Watanabe, M. Colloidal interaction in ionic liquids: Effects of ionic structures and surface chemistry on rheology of silica colloidal dispersions. Langmuir 25(2), 825-831 (2009).

35. DeFilippo, A., Zurita, M., Durth, M., Fereres, S. Rheology and microstructure of silica nanoparticle suspensions in nitrate molten salts. Book of abstracts of the 1st International Conference on Nanofluids (ICNf2019), Castelló, Spain (2019).

36. Mewis, J., Wagner, N.J. Thixotropy. Advances in Colloid and Interface Science 147–148, 214–227 (2009).

37. Amoros, J.L., Berltran, V., Sanz, V., Jarque, J.C. Electrokinetic and rheological properties of highly concentrated kaolin dispersions: influence of particle volume fraction and dispersant concentration. Applied Clay Science 49, 33-43 (2010).

38. Serrano-López, R., Fradera, J., Cuesta-López, S. Molten salts database for energy applications. Chemical Engineering and Processing 73, 87–102 (2013).

39. Kuchibhatla, A., Karakoti, A.S., Seal, S. Colloidal Stability by Surface Modification. JOM (2005) 52-56.

40. Riazi, H., Murphy, T., Webber, G.B., Atkin, R., MostafaviTehrani, S.S., Taylor, R.A. Specific Heat Control of Nanofluids: a Critical Review. International Journal of Thermal Sciences107, 25-38 (2016).